Atmos. Chem. Phys. Discuss., 12, 4679–4717, 2012
www.atmos-chem-phys-discuss.net/12/4679/2012/
doi:10.5194/acpd-12-4679-2012

Atmospheric Chemistry and Physics Discussions

Summertime photochemistry during CAREBeijing-2007: RO_x budgets and O_3 formation

Z. Liu[1], Y. Wang[1], D. Gu[1], C. Zhao[1,*], L. G. Huey[1], R. Stickel[1], J. Liao[1], M. Shao[2], T. Zhu[2], L. Zeng[2], A. Amoroso[3], F. Costabile[3], C.-C. Chang[4], and S.-C. Liu[4]

[1]School of Earth and Atmospheric Science, Georgia Institute of Technology, Atlanta, USA
[2]College of Environmental Sciences and Engineering, Peking University, Beijing, China
[3]Institute for Atmospheric Pollution, National Research Council (CNR-IIA), Rome, Italy
[4]Research Center for Environmental Changes (RCEC), Academic Sinica, Taipei, China
[*]now at: the Pacific Northwest National Laboratory, Richland, Washington, USA

Received: 23 January 2012 – Accepted: 28 January 2012 – Published: 9 February 2012

Correspondence to: Z. Liu (zhen.liu@eas.gatech.edu)

Published by Copernicus Publications on behalf of the European Geosciences Union.

Abstract

We analyze summertime photochemistry near the surface over Beijing, China, using a 1-D photochemical model (Regional chEmical and trAnsport Model, REAM-1D) constrained by in situ observations, focusing on the budgets of RO_x ($OH + HO_2 + RO_2$) radicals and O_3 formation. The daytime average of total RO_x primary production rate in Beijing is ~6.6 ppbv h^{-1}, among the highest found in urban atmospheres. The largest primary RO_x source in Beijing is photolysis of oxygenated volatile organic compounds (OVOCs), which produces HO_2 and RO_2 at average daytime rates of 2.5 ppbv h^{-1} and 1.7 ppbv h^{-1}, respectively. Photolysis of excess HONO from the unknown heterogeneous source is a predominant primary OH source at 2.2 ppbv h^{-1}, much larger than that of $O^1D + H_2O$ (0.4 ppbv h^{-1}). The largest RO_x sink is via $OH + NO_2$ reaction (1.6 ppbv h^{-1}), followed by formation of RO_2NO_2 (1.0 ppbv h^{-1}) and $RONO_2$ (0.7 ppbv h^{-1}). Due to the large aerosol surface area, aerosol uptake of HO_2 appears to be another important radical sink, although the estimate of its magnitude is highly variable depending on the reactive uptake coefficient value used. The daytime average O_3 production and loss rates are 32 ppbv h^{-1} and 6.2 ppbv h^{-1}, respectively. Assuming NO_2 to be the source of excess HONO, the NO_2 to HONO transformation leads to significant O_3 loss and reduction of its lifetime.

Our observation-based modeling analyses suggest that VOCs and heterogeneous reactions (e.g. HONO formation and aerosol uptake HO_2) play major roles in the primary radical budget and O_3 formation in Beijing. Among the VOC precursors for OVOCs, which strongly affect RO_x budgets and O_3 formation, aromatics are the largest contributor. One important ramification is that O_3 production is neither NO_x nor VOC limited, but in a transition regime, where reduction of either NO_x or VOCs could result in reduction of O_3 production. The transition regime implies more flexibility in the O_3 control strategies than a binary system of either NO_x or VOC limited regime. Further research on the spatial extent of the transition regime over the polluted eastern China is critically important for controlling regional O_3 pollution.

ACPD
12, 4679–4717, 2012

1 Introduction

Photochemical smog was first documented in 1950s in Los Angeles (Haagen-Smit and Fox, 1954), and is nowadays a prevalent air pollution phenomenon around the world (e.g., Molina and Molina, 2004; Monks, et al., 2010). A major contributor to smog is the production of secondary pollutants such as O_3 and aerosols from photochemical reactions involving NO_x ($NO_x \equiv NO + NO_2$) and volatile organic compounds (VOCs), which are emitted from various anthropogenic and natural sources. Over the past decades, continuously improving knowledge of photochemical pollution has successfully served as the basis for formulating the pollution control strategies over the United States (NRC, 1991; NARSTO, 2000). Uncertainties of photochemical modeling in some regions remain large due to the lack of accurate emission inventories (NARSTO, 2005) and incomplete knowledge of chemistry (e.g. Volkamer et al., 2010).

A region of concern is China. The rapid increasing emissions of NO_x and VOCs over China since 1980s driven by economic growth have been observed by satellites (e.g., Richter et al., 2005) and documented in bottom-up inventories (e.g., Zhang et al., 2009). As an expected consequence, elevated O_3 (e.g., Wang et al., 2006) and peroxy acetyl nitrates (PANs) (e.g., Liu et al., 2010) accompanied by high loadings of aerosols (e.g. Chan and Yao, 2008; Zhang et al., 2008) have been observed in the country. Severe O_3 and aerosol pollution on an unprecedented large regional scale (Zhao et al., 2009a; van Donkelaar et al., 2010) have also drawn attention given the large impacts on public health.

Furthermore, some recent observations over China demonstrated the complexity of photochemistry that cannot be fully explained by current knowledge. For example, surprisingly high daytime HONO concentrations from unknown sources have been observed in Beijing (An et al., 2009) and the Pearl River Delta (PRD) region (Su et al., 2008). At a suburban site over PRD, the current standard photochemistry could not explain the observed level of OH, the key oxidant in the troposphere (Hofzumahaus et al., 2009; Lu et al., 2011). Due to high loading of aerosols, heterogeneous chemistry

ACPD
12, 4679–4717, 2012

appears to be important in the radical budget (Kanaya et al., 2009) and reactive nitrogen processing (Pathak et al., 2009). A case in point is that we still do not have a clear understanding of how the large emission reductions affected secondary pollutants during the 2008 summer Beijing Olympic and Paralympic Games. Chemical transport modeling study by Yang et al. (2011) demonstrated the highly variable chemical sensitivities of O_3 to its precursor emissions due to the uncertainties in the emissions of aromatic VOCs. However, the sensitivity relationships are very difficult to derive from the observations. For example, Wang et al. (2010) found increases of O_3, sulfate and nitrate while NO_x and VOCs decreased at an urban site in Beijing in the first two weeks after emission control for the Olympics Game. Similar finding was reported at another urban site in Beijing (Chou et al., 2011). These findings reflect the fact that the effects on O_3 from precursor emission changes can be masked by the variations in the spatial pollutant distribution and meteorological conditions for dispersion, transport, and chemical photolysis.

Given the difficulty of interpreting empirical evidence, another approach is through in-depth observation-based chemical budget analyses to gain insight into the chemical system. In this work, we analyze the O_3 photochemical processes in Beijing in August 2007 during the CAREBeijing (Campaigns of Air quality REsearch in Beijing) Experiment employing the 1-D version of the Regional chEmical and trAnsport Model (REAM-1D) constrained by observed chemical species and physical parameters, including O_3, NO, PAN, HONO, VOCs, and aerosol surface areas. The goal is to gain a detailed understanding of the budgets of RO_x ($OH + HO_2 +$ organic peroxy radicals (RO_2)) radicals and formation processes of O_3 and to understand the implications on emission control strategies in Beijing and other polluted regions in China.

The remainder of the paper proceeds as follows. In Sect. 2, we describe the measurement methods and the REAM-1D model. Section 3 presents the modeling analysis results. We examine the budgets of RO_x radicals in Sect. 3.1, which will form the basis for analyzing production and loss rates of O_3 in Sect. 3.2. We then analyze the specific roles of aromatics, HONO, and aerosol uptake of HO_2 in the budgets of radicals

ACPD
12, 4679–4717, 2012

and O_3, respectively, in Sect. 3.3. We investigate the sensitivities of O_3 production to NO_x and VOCs in Sect. 3.4. In Sect. 4, we summarize our findings and discuss the implications for O_3 control strategies over China.

2 Methodology

2.1 Measurement methods

During the CAREBeijing-2007 experiment (Zhu et al., 2009), a full suite of trace gases were measured concurrently in August 2007 at an urban site located on a building roof top (~20 m a.g.l.) on the campus of Peking University (39.99° N, 116.31° E). Nitrogen monoxide (NO) was measured with a custom-made chemiluminescence detector (Ryerson et al., 2000). Total reactive nitrogen compounds (NO_y, only gas phase) were measured by the conversion of the NO_y species to NO on a molybdenum converter operated at 300 °C. PAN was measured using a chemical ionization mass spectrometer (CIMS) (Slusher et al., 2004). HONO was measured with a liquid coil scrubbing/UV–VIS instrument (Amoroso et al., 2006). O_3 and CO were measured by commercial instruments from the ECOTECH (EC9810 and EC9830). C_3–C_9 NMHCs were measured with a time resolution of 30 minutes using two online GC–FID/PID systems (Syntech Spectra GC–FID/PID GC955 series 600/800 VOC analyzer), one for the C_3–C_5 NMHCs, and the other for C_6–C_9 NMHCs (Shao et al., 2009). Another automated GC/MS/FID system was deployed to measure NMHCs in daytime (08:00–09:00 and 13:00–14:00) (Hofzumahaus et al., 2009). OVOCs were measured using the PFPH–GC/MS method (Ho and Yu, 2004). The uncertainties (1σ) for these measurements are estimated to be 5 % for NO, O_3, CO, 3–5 % for NMHCs, 10 % for NO_y, PAN, HONO and OVOCs. More detailed descriptions of the instruments and measurement methods are available in the Supplement.

ACPD
12, 4679–4717, 2012

2.2 The REAM-1D Model

The 3-D version of the Regional chEmical and trAnsport Model (REAM-3D) has been applied in a number of studies on O_3 photochemistry and transport at northern mid-latitudes (Choi et al., 2005; Wang et al., 2007; Choi et al., 2008a,b; Zhao et al., 2009a, b, 2010; Zhao and Wang, 2009; Yang et al., 2011). The REAM-1D model shares the modules for O_3-NO_x-hydrocarbon photochemistry, vertical diffusion, convective transport, and wet/dry deposition (Liu et al., 2010) with the REAM-3D model. The chemical kinetics data were updated with the latest compilation by Sander et al. (2011), and the VOC chemistry in REAM-3D is expanded to include the chemistry of aromatics based on the SAPRC-07 chemical mechanism (Carter, 2009). Vertical transport is driven by WRF assimilated meteorological fields based on the NCEP reanalysis data (Zhao et al., 2009a).

The model is constrained with measured CO, O_3, NO, HONO, NMHCs (C_2–C_9), OVOCs (acetone, acetaldehyde and formaldehyde) and aerosol surface areas and was run with a 1-min time step from 1 to 30 August 2007. The results for the last 20 days were analyzed after a spin-up time of 10 days. The REAM-1D model has been shown to be able to reproduce the observed PAN in Beijing, which is sensitive to the VOC oxidation mechanism and transport within the boundary layer (Liu et al., 2010). Our model simulated OVOCs, including formaldehyde, acetaldehyde, and acetone, agree with the observations within 20 % in terms of diurnal average concentrations, indicating that secondary production is the predominant source. Additional detailed descriptions of the REAM-1D model including VOC input and model error estimates are available in the Supplement.

Exceptionally high level of HONO was observed at daytime (~1 ppbv in the afternoon) during the study period. The gas-phase source from the NO + OH reaction alone could only explain a small portion (~10 %) of the observed HONO concentrations. We therefore introduced a pseudo-reaction of $NO_2 \rightarrow$HONO in the model in order to reproduce the observed daytime HONO and quantitatively estimate the primary radical

ACPD
12, 4679–4717, 2012

source from the heterogeneous HONO production pathway. Due to the large aerosol surface areas (~1000 μm^{-2} cm^{-3}), the uptake of HO_2 by aerosols may become a large HO_2 sink. The HO_2 aerosol reactive uptake coefficient, γ, is still quite uncertain and may be a function of temperature and aerosol composition (Thornton and Abbatt, 2005; Thornton et al., 2008; Kanaya et al., 2009; Mao et al., 2010). In this work, we use a $\gamma(HO_2) = 0.02$ in the standard model (S0 in Table 1) based on model performance in simulating PAN, and we evaluate model sensitivities by varying the value of $\gamma(HO_2)$ from 0 to 0.2 (Sect. 3.3.3).

We conducted a number of model simulations, summarized in Table 1, to understand the sensitivities of radical budgets and O_3 production to aerosol uptake of HO_2, high daytime HONO concentrations, and NO_x and VOCs. S0 is the standard model; S0a and S0b are S0 with varied $\gamma(HO_2)$ values, 0 in S0a and 0.2 in S0b, respectively. S1 is S0 without the "excess" HONO that cannot be explained by gas-phase HONO production; S2 is S0 without aromatics; S3 is S0 without excess HONO or aromatics, and S3a further removes the aerosol HO_2 uptake ($\gamma(HO_2) = 0$) in S3. The $P(O_3)_{senst}$ simulations compare O_3 production rates under varied NO_x and VOCs conditions. The $\gamma(HO_2)_{senst}$ simulations examine the sensitivities of O_3 production to different $\gamma(HO_2)$ values ranging from 0 to 0.2. In the sensitivity simulations, we did not constrain OVOCs to the observations in order to retain the feedback from OVOCs. Removing the constraint of observed OVOCs in the standard model did not lead to notable changes in RO_x concentrations or O_3 production/loss rates.

3 Results and discussions

The chemical dependence of O_3 formation on the emissions of its precursors, including NO_x and VOCs, is driven by the cycling of a variety of RO_x radicals. In this work, with the 1-D model constrained by observations of O_3 and its precursors, we first examine the abundances and budgets of RO_x radicals, and characterize the main features and uncertainties of chemistry in Beijing. Then, by focusing on the chemical pathways

ACPD
12, 4679–4717, 2012

controlling the O_3 formation, we quantitatively examine the O_3 production and loss processes and their responses to varied precursor changes, in order to understand the chemical regime of O_3 formation and its implications on O_3 control strategies.

3.1 Budgets of RO_x radicals

3.1.1 Model simulated concentrations of OH, HO_2 and RO_2

Figure 1 shows the average diurnal profiles of OH, HO_2 and RO_2 concentrations simulated in the standard model (S0). The 20-day average diurnal maximum concentrations of OH, HO_2, and RO_2 are 9×10^6, 6.8×10^8, and 4.5×10^8 molecules cm^{-3}, respectively. RO_x radical measurements over mainland China are still sparse. The maximum OH concentration (9×10^6 molecules cm^{-3}) simulated in this study for Beijing is ~50 % higher than that simulated over Mountain Tai in June of 2006 (6×10^6 molecules cm^{-3}) (Kanaya et al., 2009), and lies between the observed (13×10^6 molecules cm^{-3}) and simulated (7×10^6 molecules cm^{-3}) values at a site in PRD (Hofzumahaus et al., 2009). The maximum HO_2 concentration simulated for Beijing (6.8×10^8 molecules cm^{-3}) is close to that over Mountain Tai (Kanaya et al., 2009), and is only half of that in PRD (Hofzumahaus et al., 2009). We note that the model simulated HO_2 concentrations over China are quite sensitive to $\gamma(HO_2)$, due to the large abundance of aerosols. Removing the aerosol HO_2 sink in this study would lead to higher simulated HO_2 and OH concentrations in good agreement with the observed values at the PRD site by Hofzumahaus et al. (2009), although the locations and time of the two studies are different. Compared to urban areas outside China, the simulated OH and HO_2 concentrations for Beijing are similar to those observed in Mexico City (Shirley et al., 2006; Dusanter et al., 2009), and yet higher than those in New York City (Ren et al., 2003) and Birmingham of the UK (Emmerson et al., 2005a).

RO_2 radicals include all organic peroxy radicals derived from VOC oxidation, and they are categorized into 7 groups (Figure 1), i.e. methyl peroxy radicals (CH_3O_2), first generation peroxy radicals from alkanes ($ALKA_p$), alkenes except isoprene ($ALKE_p$),

ACPD
12, 4679–4717, 2012

isoprene (ISO_p), aromatics (ARO_p), acyl peroxy radicals (RCO_3), and peroxy radicals from OVOCs ($OVOC_p$). The most abundant 3 groups of RO_2 are CH_3O_2, AROp and RCO_3. The largest contribution of CH_3O_2 is expected. Aromatics have higher concentrations and reactivities than alkenes and alkanes (Liu et al., 2010), producing more RO_2 radicals upon oxidation. $RC(O)O_2$ radicals are produced from OH oxidation or photolysis of a variety of carbonyl compounds. $CH_3C(O)O_2$ is the simplest and most abundant $RC(O)O_2$, and also the precursor of PAN. Liu et al. (2010) showed that methylglyoxal from aromatics is the predominant source (~75 %) of $CH_3C(O)O_2$ and PAN in Beijing.

3.1.2 RO_x budgets

Figure 2 illustrates schematically the RO_x daytime (06:00 – 18:00) budgets simulated in the model. The fast RO_x cycling is driven by NO_x catelyzed VOC oxidation, which is typical in NO-rich environments (Emmerson et al., 2005b; Shirley et al., 2006; Dusanter et al., 2009; Elshorbany et al., 2009). $NO + HO_2$ (19.8 ppbv h^{-1}) and $NO + RO_2$ (12.2 ppbv h^{-1}) are the two largest pathways of radical cycling in the system, mainly due to the abundance of NO (e.g. ~5 ppbv around noontime).

It is more constructive to examine the primary sources and sinks of RO_x radicals in this relatively complex system to understand the controlling factors. Photolysis of OVOCs turns out to be the predominant primary RO_x source (4.0 ppbv h^{-1}), and is also the largest sources of HO_2 (2.4 ppbv h^{-1}) and RO_2 (1.6 ppbv h^{-1}), consistent with previous urban studies (Jenkin et al., 2000; Emmerson et al., 2005b; Dusanter et al., 2009). Photolysis of excess HONO is the second largest RO_x source (3.0–0.8 = 2.2 (ppbv h^{-1})), as well as the largest source of OH. At noontime the excess HONO produces OH at ~5 ppbv h^{-1} (Fig. 3), a rate that is comparable to that found by Su et al. (2008) at Xinken in PRD, and slightly higher than that at another site, Backgarden, in the same region (Hofzumahaus et al., 2009). However, the excess daytime HONO source strength found in China is significantly larger than most urban areas outside

ACPD
12, 4679–4717, 2012

China (e.g. Acker et al., 2006; Kleffmann, 2007 and references therein; Dusanter et al., 2009; Elshorbany et al., 2009; Costabile et al., 2010). The reasons for such a uniquely large HONO source in China are still unknown. The $O^1D + H_2O$ reaction only contributes 0.4 ppbv h^{-1} of primary OH production. Summing up all these aforementioned sources gives a total primary RO_x production rate at 6.6 ppbv h^{-1} (2.6 ppbv h^{-1} for OH, 2.4 ppbv h^{-1} for HO_2, and 1.6 ppbv h^{-1} for RO_2), which is comparable to that in Santiago of Chile (7.0 ppbv h^{-1}) (Elshorbany et al., 2009), but ~50 % higher than those in Mexico City in 2006 (4.75 ppbv h^{-1}) (Dusanter et al., 2009), and Birmingham of the UK (4.5 ppbv h^{-1}) (Emmerson et al., 2005b).

RO_x radicals are removed ultimately from the atmosphere via deposition of radical reservoir species, e.g. HNO_3, H_2O_2, ROOH. The net radical losses via NO_x-radical reactions are 3.6 ppbv h^{-1}, including $NO_2 + OH$ producing HNO_3 (1.7 ppbv h^{-1}), $RO_2 + NO_2$ reaction producing organic peroxy nitrates (RO_2NO_2, mostly PANs) (1.1 ppbv^{-1}), and $RO_2 + NO$ reaction producing organic nitrates ($RONO_2$) (0.8 ppbv h^{-1}). By contrast, the radical loss rates via radical-radical reactions producing peroxides such as H_2O_2 and ROOH are much lower (0.6 ppbv h^{-1} in total). Such a contrast has been typically seen as a feature of chemistry in NO_x-rich urban environments. Another important and yet uncertain RO_x sink in Figs. 2 and 3 is the aerosol uptake of HO_2 (1.1 ppbv h^{-1}), mainly owing to abundant aerosols in Beijing. The magnitude of this radical sink varies significantly with values of $\gamma(HO_2)$ used in the model (Sect. 3.3.3).

It is also noteworthy that the two $RO_2 + NO_x$ reaction pathways collectively contribute a net RO_x loss at 1.9 ppbv h^{-1}, larger than that of $NO_2 + OH$ (1.6 ppbv h^{-1}), which is different from most urban environments outside China (Emmerson et al., 2005b; Dusanter et al., 2009; Elshorbany et al., 2009). Figure 4 shows the diurnal transition of RO_2NO_2 production and loss. During most of the daytime, RO_2NO_2 production dominates over its loss processes (mainly via thermal decomposition) leading to the net formation of RO_2NO_2 and thus sequestering of NO_2 and $R(O)O_2$ radicals. RO_2NO_2

ACPD
12, 4679–4717, 2012

loss starts to dominate over production from the late afternoon into the evening. Such a diurnal transition of RO_2NO_2 production and loss differs from the often used steady-state assumption of RO_2NO_2, and has significant impacts on O_3 production (Sect. 3.2). $RONO_2$ is formed from minor channels in NO + RO_2 reactions, and the importance of this channel is known to be a function of the size of RO_2. $RONO_2$ has longer lifetimes (at least 2 days) than RO_2NO_2, and its loss by transport and deposition is a net loss of RO_x radicals.

Another feature in the chemical system in Fig. 2 is the coupling of NO_x and VOCs chemistry. Both are involved in major RO_x primary sources, i.e. $NO_2 \rightarrow$HONO$\rightarrow$OH (2.2 ppbv h^{-1}) and photolysis of OVOCs (4.2 ppbv h^{-1}). Meanwhile, some of the RO_x sinks, i.e. RO_2 + NO/NO_2 also depend on both NO_x and VOCs, rather than only one of them. These aspects of chemistry have implications for O_3 sensitivities to NO_x and VOCs (Farmer et al., 2011). In Sect. 3.2–3.3, we examine the formation of O_3, and its sensitivities to various factors, including excess HONO, aromatics, $\gamma(HO_2)$, as well as NO_x and VOCs.

3.2 O_3 photochemistry

3.2.1 O_3 production and loss rates

The formation of O_3 in the troposphere is via the reactions of NO and peroxy radicals. On the other hand, due to the fast cycling of O_3 and NO_2 under urban conditions, O_3 loss is due to a number of reactions leading to the destruction of O_3 and NO_2. The daytime average $P(O_3)$ as the sum of HO_2 + NO (19.8 ppbv h^{-1}) and RO_2 + NO (12.2 ppbv h^{-1}) is 32 ppbv h^{-1} (Fig. 2), comparable to previous calculations for Beijing (Lu et al., 2011), and is near the top of reported values for urban environments (e.g. Ren et al., 2003; Shirley et al., 2006; Kanaya et al., 2008; Wood et al., 2009). The reaction of HO_2 + NO accounts for roughly 2/3 of $P(O_3)$. RCO_3 + NO, CH_3O_2 + NO and AROp + NO are the predominant RO_2 + NO reactions, due to the relative abundance of RO_2 radicals (Fig. 1) and the larger reaction rate constant of RCO_3 + NO. The mean

ACPD
12, 4679–4717, 2012

daytime peak of $P(O_3)$ is ~60 ppbv h^{-1}, occurring around 11:00 (Fig. 5), earlier than the peaks of both HO_2 and RO_2 around 13:00 because of the decrease NO concentrations from morning to early afternoon. $P(O_3)$ is also found to peak around 10:00–11:00 local time in Mexico City (Shirley et al., 2006).

The daytime mean and maximum $L(O_3)$ rates are 6.2 ppbv h^1 and 12 ppbv h^{-1}, respectively, roughly 1/5 of $P(O_3)$. $L(O_3)$ consists of $NO_2 \rightarrow$HONO (2.2 ppbv h^{-1}), $NO_2 + OH$ (1.7 ppbv h^{-1}), $RO_2 + NO_2$ (1.1 ppbv h^{-1}), $O^1D + H_2O$ (0.4 ppbv h^{-1}), and other minor reactions. Given the noontime O_3 and NO_2 concentrations (~55 ppbv and ~10 ppbv) and the loss rate of O_3, the chemical lifetime of O_3 is ~5 h. It is interesting that the unknown source of HONO from NO_2 also serves as a $L(O_3)$ term, and is in fact the most important $L(O_3)$ reaction (~40 %), directly affecting O_3 formation and the lifetime of O_3. The average daytime net formation rate of O_3, i.e. $P(O_3) - L(O_3)$, is ~26 ppbv h^{-1}.

3.2.2 O_3 production efficiency

Alongside O_3 formation, NO_x is transformed into oxidized nitrogen compounds NO_z ($NO_z \equiv NO_y$-NO_x), e.g. $RONO_2$, RO_2NO_2, and HNO_3, and then eventually removed from the atmosphere by deposition. NO_z compounds at daytime account for 20-50 % of total NO_y (Fig. 6). The O_3 production efficiency (OPE) of NO_x is defined as the amount of O_3 produced during the lifetime of NO_x (Liu et al., 1987). Based on our model calculated $P(O_3)$ and $P(NO_z)$ (Fig. 2), we estimate a daytime average OPE to be 9.7, which is much larger than that estimated by Wang et al. (2010) for the summer of 2008, and yet within the estimates by Chou et al. (2011) for the summer of 2006. It is also within the estimated range for Mexico City (4–12) (Lei et al., 2007; Wood et al., 2009). Considering the moderate concentrations of HO_2 and RO_2 compared to other urban environments, the relatively high OPE from our calculation is mainly due to the high daytime NO concentration (~5 ppbv at noontime).

ACPD
12, 4679–4717, 2012

3.3 Sensitivity studies – assessing the impacts of HONO, aromatics and aerosol uptake of HO_2

Based on the results from standard model (S0) results discussed above, we found that excess HONO, reactive aromatic VOCs, and aerosol uptake of HO_2 are important factors in the photochemical system in Beijing. In next section, we extend our analyses of these individual factors by comparing results from a series of sensitivity simulations listed in Table 1.

3.3.1 Impacts of excess HONO on RO_x budgets and O_3 formation

The large net OH source from the photolysis of excess HONO relative to the other primary OH sources has been shown in Fig. 2. Figure 7 shows the sensitivity simulation results without excess HONO (S1). The standard model (S0) has ~60 % higher daytime average OH concentration than S1 due to the excess HONO. Increased OH leads to more active photochemistry and thus ~50 % increases of HO_2 and RO_2 concentrations, as well as $P(O_3)$. A second consequence is the large sink (~40 %) of O_3 due to excess HONO production (Sect. 3.2). The impact of excessive HONO is even larger (~130 %) when aromatics are not included (comparing S3 to S2 in Fig. 7). This excess HONO term is usually not considered in the budget of O_3 in previous studies. For locations like Beijing, it appears necessary to take into account the production and loss of O_3 due to excess HONO. More importantly, the nature of excess HONO is currently unknown and needs to be considered as a major source of uncertainty for understanding O_3. We note that the daytime HONO concentrations measured in this and other studies over China (e.g. Su et al., 2008), i.e. roughly 1 ppbv on average during daytime, are substantially higher than studies elsewhere. Therefore, our finding of the important role of excess HONO should suffer much less from the instrument uncertainties than studies outside China (e.g. Pinto et al., 2010). The large abundance of HONO actually makes polluted regions over China a uniquely ideal place for quantitative studying HONO sources and chemistry.

ACPD
12, 4679–4717, 2012

3.3.2 Direct and secondary impacts from aromatics

Aromatics are the most reactive and abundant VOC group measured in Beijing (Liu et al., 2010). The direct impact of aromatics on radical budgets and O_3 formation is via contributing first generation RO_2 (AROp) upon oxidation by OH; and we refer the effect due to subsequent oxidation products as secondary. Comparing the results of S0 to S2 (Fig. 7), adding aromatics leads to a factor of 2 increase of HO_2, RO_2, and $P(O_3)$. These changes obviously could not be explained solely by the addition of AROp radicals (Fig. 5). Careful inspection of the model results shows that OVOCs concentrations increase drastically (by 50 %–80 %) after adding aromatics, and their photolysis further produces substantial amounts of primary RO_2 and HO_2. More significantly, the presence of aromatics in S0 increases OH by ~30 % compared to S2 despite of the loss of OH by reacting with aromatics. Therefore, the overall increase of primary RO_x production from the secondary impact by aromatics is large enough to compensate for the shift from OH to peroxy radicals in the RO_x family. If the reactions of excess HONO are not included, the impacts by aromatics (from S3 to S1) are even more drastic, leading to more than 100 % increase of HO_2, RO_2 and $P(O_3)$, and 50 % increase of OH. We note that the finding on the significance of aromatics VOCs on photochemistry is qualitatively robust. However, the quantitative results presented here depend on the chemical mechanism used for aromatic VOC oxidation, for example, the yields of dicarbonyls, which are uncertain (e.g. Carter, 2009). In situ measurements of OVOC species, especially those dicarbonyls, such as methylglyoxal and glyoxal, will be needed to further constrain the model.

3.3.3 Aerosol uptake of HO_2

Figure 8 shows the variations of daytime average HO_2, OH concentrations and $P(O_3)$ rates as a function of $\gamma(HO_2)$. HO_2 concentration drops by about ~60 % from 4.05×10^8 molecules cm^{-3} at $\gamma(HO_2) = 0$ to 1.65×10^8 molecules cm^{-3} at $\gamma(HO_2) = 0.2$. Correspondingly, $P(O_3)$ decreases by ~50 % from 35.4 ppbv h^{-1} to 23.3 ppbv h^{-1}, and

ACPD
12, 4679–4717, 2012

OH drops by 30 % from 5.26×10^6 molecules cm^{-3} to 3.65×10^6 molecules cm^{-3}. $P(O_3)$ and OH changes are not as large as HO_2 in part because the impact of $\gamma(HO_2)$ on RO_2 radicals is indirect and not as large. Figure 8 suggests that $\gamma(HO_2)$ is a large source of uncertainty in current HO_x simulation studies over pollute regions of China, where aerosol loading is high (Kanaya et al., 2009).

3.4 Chemical regimes of O_3 production

We diagnose the $P(O_3)$ chemical regimes in Beijing using two approaches. First, we examine the sensitivity of $P(O_3)$ to perturbations of NO and VOC concentrations; we also try to use previously proposed diagnostic equations (e.g. Sillman et al. , 1990; Kleinman et al., 1997; Daum et al., 2000) for NO_x-limited and VOC-limited regimes, as has been done in previous studies (Lei et al., 2007). Since the chemical environment in Beijing is strongly affected various factors, e.g. excess HONO, aromatics, and aerosol uptake of HO_2, not presented in the US where those previous theoretical studies (e.g. Sillman et al., 1990; Kleinman et al., 1997) were conducted, we analyze all the scenarios listed in Table 1 and then discuss the possible impacts from those factors on $P(O_3)$ chemical regimes in Beijing.

3.4.1 Sensitivity simulation results

In the sensitivity analyses (Table 1), we vary NO and VOCs concentrations (110 %, 90 %, 70 %, and 50 % of the observed values) and examine the change of $P(O_3)$, i.e. $\Delta P(O_3)$. $P(O_3)$ consistently show positive responses to ΔNO, i.e. an increase of NO leads to an increase of $P(O_3)$, although the former is always larger than the latter, i.e., the $\Delta P(O_3) - \Delta NO$ lines are to the left of the 1:1 line (Fig. 9a). $P(O_3)$ is largely determined by the product of NO and HO_2 (RO_2) concentrations. The non-linear dependence of $P(O_3)$ on NO is a reflection of the dependence of HO_2 and RO_2 on NO. For example, increasing NO leads to decreased peroxy radicals due in part to the conversion of peroxy radicals to OH and RO by reacting with NO; the degree of peroxy

ACPD
12, 4679–4717, 2012

radical decrease is also a function of the change in primary RO_x sources and sinks. Comparing scenarios without aromatics and HONO (S3 and S3a) with those with both or either one of them (S0, S1 or S2), $P(O_3)$ in the former scenarios (S3 and S3a) is much less sensitive to ΔNO (e.g., the flat shapes of the orange lines in Fig. 9a). The larger sensitivity of peroxy radicals to NO change in S3 and S3a is because of a much smaller primary RO_x source without excess HONO or aromatics or both (Sect. 3.3). Similarly, inspection of the difference between S0 and S0a or among S3, S3a and S3b shows that a larger HO_2 aerosol sink leads to a lesser sensitivity of peroxy radicals to NO and hence a higher sensitivity of $P(O_3)$ to NO.

The complexity of the $P(O_3)$-NO sensitivity also results in part from the change over the course of a day (Fig. 10). Generally, $P(O_3)$ shows a larger sensitivity to NO in the afternoon than in the morning. Under different scenarios, such as S0 and S3a in Fig. 10, $P(O_3)$-NO sensitivities show different transitions over the course of daytime. This daytime transition of $P(O_3)$-NO sensitivity is due to the fast decreasing NO_x from the morning towards the afternoon and thus reducing the importance of NO_x in sequestering radicals, while the primary RO_x source increases into the afternoon.

In contrast to the largely varying degrees of sensitivities of $P(O_3)$ to NO, the sensitivity of PO_3 to VOCs is much more uniform and closer to the 1:1 linear response (Fig. 9b). The largest deviation from the 1:1 response line is the simulation without aromatics (S2) due to the large impact of aromatics to primary RO_x sources (Sect. 3.3.2). Figure 9a and 9b show that the $P(O_3)$-VOC response resembles the VOC-limited chemical regime (Sillman et al., 1990), although the $P(O_3)$-NO response does not, suggesting that photochemical O_3 production in Beijing is neither NO_x-limited nor VOC-limited, but lies in a transition regime where reduction of both can reduce $P(O_3)$.

Concurrent reduction of NO and VOC concentrations leads to greater $P(O_3)$ reduction than reducing either (Fig. 9c), although the additional reduction from VOC-reduction only scenarios (Fig. 9d) varies. In agreement with the $P(O_3)$-NO sensitivity (Fig. 9a), the least change from the VOC-only scenarios is from the simulations S3 and S3a in which neither excess HONO nor aromatics is included.

ACPD
12, 4679–4717, 2012

An important implication from Fig. 9 is that concurrent reduction of both NO and VOCs only gives limited additional $P(O_3)$ reduction than reducing one of them. For example, $\Delta P(O_3)_{NO+VOCs}$ from 50 % reductions of both NO and VOC is only 20 % more than $\Delta P(O_3)_{VOCs}$ of 50 % reduction in VOC (Fig. 9d for S1b). Under the most likely scenario (with excess HONO and aromatics) based on the in situ observations, reducing either NO_x or VOCs can be effective while reducing both may not bring enough air quality benefits to justify the social-economic costs.

3.4.2 Evaluation with diagnostic equations of O_3 production for different chemical regimes

Various studies have provided easier diagnostics on O_3 production regimes (e.g. Sillman et al., 1990; Kleinman et al., 1997; Daum et al., 2000). Lei et al. (2007) summarized these studies into two equations:

$$NO_x - \text{limited regime}, P(O_3) = Y \frac{k_t}{\sqrt{2k_{eff}}} \sqrt{Q - L_N - L_R}[NO] \quad (1)$$

$$VOC - \text{limited regime}, P(O_3) = Y \frac{L_{OH-VOC}}{L_{OH-NO_2}} (Q - 2PER - L_R - L_{ON}) \quad (2)$$

where k_t is the weighted average rate constant for reaction of HO_2 and RO_2 with NO; k_{eff} is the effective rate constant for peroxide (H_2O_2 and ROOH) formation; Q is the total primary source of RO_x radicals, in ppbv h^{-1}; L_N, L_R and L_{ON} are the radical loss rates due to the reactions of $OH + HO_2$, $RO_2 + R'O_2$, and radical-NO_x reactions excluding $OH + NO_2$, respectively; Y is the average yield of HO_2 and RO_2 for each OH + VOC reaction; L_{OH-VOC} and L_{OH-NO_2} are the loss rates of OH due to reactions with VOCs and NO_2, respectively; PER is the peroxide formation rate.

We compare the correlations between model calculated hourly $P(O_3)$ (ppbv h^{-1}) and those from the diagnostic equations (Lei et al., 2007). The results for different model

ACPD
12, 4679–4717, 2012

sensitivity simulations are shown in Table 2. We also show in Table 2 the correlations with NO and the primary RO_x source Q. In the standard model (S0), $P(O_3)$ shows better correlation with $\frac{L_{OH-VOC}}{L_{OH-NO_2}}(Q-2PER-L_R-L_{ON})$ (afternoon $R^2=0.79$; daytime $R^2=0.79$) than with the NO_x-limited diagnostics ($\sqrt{Q-L_N-L_R}[NO]$) (afternoon $R^2=0.50$; daytime $R^2=0.19$), mainly due to the much better $P(O_3)$-Q correlation (afternoon $R^2=0.66$; daytime $R^2=0.74$) than the $P(O_3)$-NO correlation (afternoon $R^2=0.22$; daytime $R^2=0.002$). These suggest that $P(O_3)$ during our observations in Beijing behave more like in the VOC-limited regime than the NO_x-limited regime. This is particularly true when morning data are taken into account since O_3 production can clearly reside in the VOC-limited regime (Fig. 10). In the afternoon when O_3 production is large, however, both diagnostics show reasonably good correlations with the $P(O_3)$. An outlier is the scenario of S2 when aromatics are not included; the chemical regime clearly shifts into the VOC-limited regime given the much better correlation ($R^2=0.79$) with $\frac{L_{OH-VOC}}{L_{OH-NO_2}}(Q-2PER-L_R-L_{ON})$ than with $\sqrt{Q-L_N-L_R}[NO]$ ($R^2=0.26$). In the scenario of S0a (without HO_2 aerosol uptake) for the afternoon, $P(O_3)$ correlate even better with the NO_x-limited diagnostics ($R^2=0.56$) than with the VOC-limited diagnostics ($R^2=0.49$). Comparing the results of S0, S0a, and S0b, aerosol uptake of HO_2 tends to shift the O_3 production more towards the VOC-limited regime.

In general, the diagnostic equations are consistent with our sensitivity simulations, suggesting that under the most realistic scenario (S0), O_3 production in Beijing is in the transition regime. Aromatics and excess HONO tend to shift O_3 production into NO_x-limited regime, while aerosol HO_2 sink tends to shift it towards VOC-limited regime.

4 Conclusions

Through a detailed chemical budget analysis, we find that summertime photochemistry in Beijing is driven by fast formation, recycling and removal of RO_x radicals. The

ACPD
12, 4679–4717, 2012

total RO_x primary source (and sink) (6.6 ppbv h^{-1}) in Beijing is close to the largest values reported for urban environments. Photolysis of OVOCs (4.2 ppbv h^{-1}) and excess HONO (2.2 ppbv h^{-1}) are the two largest RO_x sources, much more important than that from $O^1D + H_2O$ (0.4 ppbv h^{-1}). Formation of RO_2NO_2 (1.0 ppbv h^{-1}) and $RONO_2$ (0.7 ppbv h^{-1}) are as important as the typical major RO_x sink via $OH+NO_2$ reaction (1.6 ppbv h^{-1}). Aromatics are the major player in OVOC and organic nitrate formation. Aerosol uptake of HO_2 may also be a major RO_x sink due to the large aerosol surface area in Beijing, although this sink is quite sensitive to the value of $\gamma(HO_2)$. The importance of aromatics, heterologous HONO production, and possibly large aerosol update of HO_2 signifies the unique photochemical environments in Beijing. These characteristics are likely to be present over many regions of the polluted eastern China with large clusters of cities and industrial regions. Observation-based modeling studies of RO_x radical chemistry over these regions by including high quality comprehensive measurements of RO_x radicals, HONO, organic nitrates, and VOCs (aromatics in particular) and their oxidation products will be necessary to reduce the uncertainties of the factors discussed in this study and develop more accurate quantitative understanding of the chemical system.

The chemical production of O_3 in Beijing is extremely fast, at 32 ppbv h^{-1} on average during daytime. The high concentrations of NO (~5 ppbv at noontime), excess HONO and aromatic VOCs are the major driving factors. The chemical loss of O_3 is also fast, about 6 ppbv h^{-1}, and the heterogeneous formation of excess HONO via $NO_2 \rightarrow$HONO is actually the largest (~40 %) O_3 loss term. Sensitivity simulations and analysis using diagnostic equations suggest that the O_3 production in Beijing does not lie in either the VOC-limited regime or in the NO_x-limited regime, but in the transition regime, where reduction of either NO_x or VOCs could lead to reduced O_3 production. In the transition regime, the co-benefit of concurrent reduction of both NO_x and VOCs is small, which may not bring enough air quality benefits to justify the social-economic costs. However, it also implies that there is flexibility in choosing either NO_x or VOC reduction to achieve the most cost-effective O_3 reduction.

ACPD
12, 4679–4717, 2012

In this study, we have focused on understanding the photochemistry using observation-constrained modeling. Our results point to the chemical characteristics not yet well represented in current 3-D modeling studies. The large clustering of concentrated city and industrial regions in the eastern China, such as North China Plain (NCP), Yangtze River Delta (YRD), and PRD, would suggest that fast photochemistry plays a critically important role in determining O_3 levels in these regions. 3-D modeling analysis, ideally constrained by in situ or remote sensing observations, will be necessary to understand the interplay of chemistry and transport on the regional and global scales.

Supplementary material related to this article is available online at: http://www.atmos-chem-phys-discuss.net/12/4679/2012/acpd-12-4679-2012-supplement.pdf.

Acknowledgements. This work was supported by the National Science Foundation Atmospheric Chemistry Program.

References

Acker, K., Febo, A., Trick, S., Perrino, C., Bruno, P., Wiesen, P., Moller, D., Wieprecht, W., Auel, R., Giusto, M., Geyer, A., Platt, U., and Allegrini, I.: Nitrous acid in the urban area of Rome, Atmos. Environ., 40, 3123–3133, doi:10.1016/j.atmosenv.2006.01.028, 2006.

Amoroso, A., Beine, H. J., Sparapani, R., Nardino, M., and Allegrini, I.: Observation of coinciding arctic boundary layer ozone depletion and snow surface emissions of nitrous acid, Atmos. Environ., 40, 1949–1956, 2006.

An, J. L., Zhang, W., and Qu, Y.: Impacts of a strong cold front on concentrations of HONO, HCHO, O_3, and NO_2 in the heavy traffic urban area of Beijing, Atmos. Environ., 43, 3454–3459, doi:10.1016/j.atmosenv.2009.04.052, 2009.

Carter, W. P. L.: Development of the SAPRC–07 chemical mechanism and upadated ozone

ACPD
12, 4679–4717, 2012

reactivity scales. Final Report to the California Air Resources Board Contract no. 03–318, 2009.
Cermak, J. and Knutti, R.: Beijing Olympics as an aerosol field experiment, Geophys. Res. Lett., 36, L10806, doi:10.1029/2009gl038572, 2009.
Chan, C. K. and Yao, X.: Air pollution in mega cities in China, Atmos. Environ., 42, 1–42, doi:10.1016/j.atmosenv.2007.09.003, 2008.
Choi, Y., Wang, Y. H., Zeng, T., Martin, R. V., Kurosu, T. P., and Chance, K.: Evidence of lightning NO_x and convective transport of pollutants in satellite observations over North America, Geophys. Res. Lett., 32, L02805, doi:10.1029/2004gl021436, 2005.
Choi, Y., Wang, Y., Zeng, T., Cunnold, D., Yang, E. S., Martin, R., Chance, K., Thouret, V., and Edgerton, E.: Springtime transitions of NO_2, CO, and O_3 over North America: Model evaluation and analysis, J. Geophys. Res.-Atmos., 113, D20311, doi:10.1029/2007jd009632, 2008a.
Choi, Y., Wang, Y. H., Yang, Q., Cunnold, D., Zeng, T., Shim, C., Luo, M., Eldering, A., Bucsela, E., and Gleason, J.: Spring to summer northward migration of high O-3 over the western North Atlantic, Geophys. Res. Lett., 35, L04818, doi:10.1029/2007gl032276, 2008b.
Chou, C. C. K., Tsai, C. Y., Shiu, C. J., Liu, S. C., and Zhu, T.: Measurement of NO_y during Campaign of Air Quality Research in Beijing 2006.
CAREBeijing-2006: Implications for the ozone production efficiency of NO_x, J. Geophys. Res.-Atmos., 114, D00g01, doi:10.1029/2008jd010446, 2009.
Chou, C. C. K., Tsai, C. Y., Chang, C. C., Lin, P. H., Liu, S. C., and Zhu, T.: Photochemical production of ozone in Beijing during the 2008 Olympic Games, Atmos. Chem. Phys., 11, 9825–9837, doi:10.5194/acp-11-9825-2011, 2011.
Costabile, F., Amoroso, A., and Wang, F.: Sub-mu m particle size distributions in a suburban Mediterranean area. Aerosol populations and their possible relationship with HONO mixing ratios, Atmos. Environ., 44, 5258–5268, doi:10.1016/j.atmosenv.2010.08.018, 2010.
Daum, P. H., Kleinman, L. I., Imre, D. G., Nunnermacker, L. J., Lee, Y.-N., Springston, S. R., Newman, L., and Weinstein-Lloyd, J.: Analysis of the processing of Nashville urban emissions on July 3 and July 18, 1995, J. Geophys. Res., 105, 9155–9164, 2000.
Dusanter, S., Vimal, D., Stevens, P. S., Volkamer, R., Molina, L. T., Baker, A., Meinardi, S., Blake, D., Sheehy, P., Merten, A., Zhang, R., Zheng, J., Fortner, E. C., Junkermann, W., Dubey, M., Rahn, T., Eichinger, B., Lewandowski, P., Prueger, J., and Holder, H.: Measurements of OH and HO2 concentrations during the MCMA-2006 field campaign – Part 2:

ACPD
12, 4679–4717, 2012

Model comparison and radical budget, Atmos. Chem. Phys., 9, 6655–6675, doi:10.5194/acp-9-6655-2009, 2009.
Elshorbany, Y. F., Kurtenbach, R., Wiesen, P., Lissi, E., Rubio, M., Villena, G., Gramsch, E., Rickard, A. R., Pilling, M. J., and Kleffmann, J.: Oxidation capacity of the city air of Santiago, Chile, Atmos. Chem. Phys., 9, 2257–2273, doi:10.5194/acp-9-2257-2009, 2009.
Emmerson, K. M., Carslaw, N., Carpenter, L. J., Heard, D. E., Lee, J. D., and Pilling, M. J.: Urban atmospheric chemistry during the PUMA campaign 1: Comparison of modelled OH and HO_2 concentrations with measurements, J. Atmos. Chem., 52, 143–164, doi:10.1007/s10874-005-1322-3, 2005a.
Emmerson, K. M., Carslaw, N., and Pilling, M. J.: Urban atmospheric chemistry during the PUMA campaign 2: Radical budgets for OH, HO_2 and RO_2, J. Atmos. Chem., 52, 165–183, doi:10.1007/s10874-005-1323-2, 2005b.
Farmer, D. K., Perring, A. E., Wooldridge, P. J., Blake, D. R., Baker, A., Meinardi, S., Huey, L. G., Tanner, D., Vargas, O., and Cohen, R. C.: Impact of organic nitrates on urban ozone production, Atmos. Chem. Phys., 11, 4085–4094, doi:10.5194/acp-11-4085-2011, 2011.
Haagen-Smit, A. J. and Fox, M. M.: Photochemical ozone formation with hydrocarbons and automobile exhaust, Japca J. Air Waste Ma., 4, 105–109, 1954.
Hecobian, A., Liu, Z., Hennigan, C. J., Huey, L. G., Jimenez, J. L., Cubison, M. J., Vay, S., Diskin, G. S., Sachse, G. W., Wisthaler, A., Mikoviny, T., Weinheimer, A. J., Liao, J., Knapp, D. J., Wennberg, P. O., Krten, A., Crounse, J. D., Clair, J. St., Wang, Y., and Weber, R. J.: Comparison of chemical characteristics of 495 biomass burning plumes intercepted by the NASA DC-8 aircraft during the ARCTAS/CARB-2008 field campaign, Atmos. Chem. Phys., 11, 13325–13337, doi:10.5194/acp-11-13325-2011, 2011.
Ho, S. S. H., and Yu, J. Z.: Determination of airborne carbonyls: Comparison of a thermal desorption/GC method with the standard DNPH/HPLC method, Environ. Sci. Technol., 38, 862–870, doi:10.1021/es034795w, 2004.
Hofzumahaus, A., Rohrer, F., Lu, K. D., Bohn, B., Brauers, T., Chang, C. C., Fuchs, H., Holland, F., Kita, K., Kondo, Y., Li, X., Lou, S. R., Shao, M., Zeng, L. M., Wahner, A., and Zhang, Y. H.: Amplified Trace Gas Removal in the Troposphere, Science, 324, 1702–1704, doi:10.1126/science.1164566, 2009.
Jenkin, M. E. and Clemitshaw, K. C.: Ozone and other secondary photochemical pollutants: chemical processes governing their formation in the planetary boundary layer, Atmos. Environ., 34, 2499–2527, doi:10.1016/s1352-2310(99)00478-1, 2000.

ACPD
12, 4679–4717, 2012

Kanaya, Y., Fukuda, M., Akimoto, H., Takegawa, N., Komazaki, Y., Yokouchi, Y., Koike, M., and Kondo, Y.: Urban photochemistry in central Tokyo: 2. Rates and regimes of oxidant ($O_3 + NO_2$) production, J. Geophys. Res.-Atmos., 113, D06301, doi:10.1029/2007jd008671, 2008.

Kanaya, Y., Pochanart, P., Liu, Y., Li, J., Tanimoto, H., Kato, S., Suthawaree, J., Inomata, S., Taketani, F., Okuzawa, K., Kawamura, K., Akimoto, H., and Wang, Z. F.: Rates and regimes of photochemical ozone production over Central East China in June 2006: a box model analysis using comprehensive measurements of ozone precursors, Atmos. Chem. Phys., 9, 7711–7723, doi:10.5194/acp-9-7711-2009, 2009.

Kleffmann, J.: Daytime sources of nitrous acid (HONO) in the atmospheric boundary layer, ChemPhysChem, 8, 1137-1144, 10.1002/cphc.200700016, 2007.

Kleinman, L. I., Daum, P. H., Lee, J. H., Lee, Y.-N., Nunnermacker, L. J., Springston, S. R., Newman, L., Weinstein-Lloyd, J., and Sillman, S.: Dependence of ozone production on NO and hydrocarbons in the troposphere, Geophys. Res. Lett., 24, 2299–2302, 1997.

Lei, W., de Foy, B., Zavala, M., Volkamer, R., and Molina, L. T.: Characterizing ozone production in the Mexico City Metropolitan Area: a case study using a chemical transport model, Atmos. Chem. Phys., 7, 1347–1366, doi:10.5194/acp-7-1347-2007, 2007.

Liu, S. C., Trainer, M., Fehsenfeld, F. C., Parrish, D. D., Williams, E. J., Fahey, D. W., Hübler, G., and Murphy, P. C.: Ozone Production in the Rural Troposphere and the Implications for Regional and Global Ozone Distributions, J. Geophys. Res., 92, 4191–4207, 1987.

Liu, Z., Wang, Y. H., Gu, D. S., Zhao, C., Huey, L. G., Stickel, R., Liao, J., Shao, M., Zhu, T., Zeng, L. M., Liu, S. C., Chang, C. C., Amoroso, A., and Costabile, F.: Evidence of Reactive Aromatics As a Major Source of Peroxy Acetyl Nitrate over China, Environ. Sci. Technol., 44, 7017–7022, doi:10.1021/es1007966, 2010.

Lou, S., Holland, F., Rohrer, F., Lu, K., Bohn, B., Brauers, T., Chang, C. C., Fuchs, H., Häseler, R., Kita, K., Kondo, Y., Li, X., Shao, M., Zeng, L., Wahner, A., Zhang, Y., Wang, W., and Hofzumahaus, A.: Atmospheric OH reactivities in the Pearl River Delta – China in summer 2006: measurement and model results, Atmos. Chem. Phys., 10, 11243–11260, doi:10.5194/acp-10-11243-2010, 2010.

Lu, K. D., Rohrer, F., Holland, F., Fuchs, H., Bohn, B., Brauers, T., Chang, C. C., Häseler, R., Hu, M., Kita, K., Kondo, Y., Li, X., Lou, S. R., Nehr, S., Shao, M., Zeng, L. M., Wahner, A., Zhang, Y. H., and Hofzumahaus, A.: Observation and modelling of OH and HO_2 concentrations in the Pearl River Delta 2006: a missing OH source in a VOC rich atmosphere, Atmos. Chem.

ACPD
12, 4679–4717, 2012

Phys. Discuss., 11, 11311–11378, doi:10.5194/acpd-11-11311-2011, 2011.
Mao, J., Jacob, D. J., Evans, M. J., Olson, J. R., Ren, X., Brune, W. H., Clair, J. M. S., Crounse, J. D., Spencer, K. M., Beaver, M. R., Wennberg, P. O., Cubison, M. J., Jimenez, J. L., Fried, A., Weibring, P., Walega, J. G., Hall, S. R., Weinheimer, A. J., Cohen, R. C., Chen, G., Crawford, J. H., Jaegl, L., Fisher, J. A., Yantosca, R. M., Le Sager, P., and Carouge, C.: Chemistry of hydrogen oxide radicals (HO_x) in the Arctic troposphere in spring, Atmos. Chem. Phys. Discuss., 10, 6955–6994, doi:10.5194/acpd-10-6955-2010, 2010.
Molina, M. J. and Molina, L. T.: Megacities and atmospheric pollution, J. Air Waste Manage. Assoc., 54, 644–680, 2004.
Monks, P. S., Granier, C., Fuzzi, S., Stohl, A., Williams, M. L., Akimoto, H., Amann, M., Baklanov, A., Baltensperger, U., Bey, I., Blake, N., Blake, R. S., Carslaw, K., Cooper, O. R., Dentener, F., Fowler, D., Fragkou, E., Frost, G. J., Generoso, S., Ginoux, P., Grewe, V., Guenther, A., Hansson, H. C., Henne, S., Hjorth, J., Hofzumahaus, A., Huntrieser, H., Isaksen, I. S. A., Jenkin, M. E., Kaiser, J., Kanakidou, M., Klimont, Z., Kulmala, M., Laj, P., Lawrence, M. G., Lee, J. D., Liousse, C., Maione, M., McFiggans, G., Metzger, A., Mieville, A., Moussiopoulos, N., Orlando, J. J., O'Dowd, C. D., Palmer, P. I., Parrish, D. D., Petzold, A., Platt, U., Pöschl, U., Prevot, A. S. H., Reeves, C. E., Reimann, S., Rudich, Y., Sellegri, K., Steinbrecher, R., Simpson, D., ten Brink, H., Theloke, J., van der Werf, G. R., Vautard, R., Vestreng, V., Vlachokostas, C., and von Glasow, R.: Atmospheric composition change – global and regional air quality, Atmos. Environ., 43, 5268–5350, doi:10.1016/j.atmosenv.2009.08.021, 2009.
NARSTO: An assessment of tropospheric ozone pollution – A North American perspective. NARSTO Management Office (Envair), Pasco, Washington, http://narsto.org/, 2000.
NARSTO: Improving emission inventories for effective Air Quality Management Across North America, NARSTO 05–001, Pasco, Washington, USA, 2005.
NRC (National Research Council): Rethinking the ozone problem in urban and regional air pollution, National Academy Press, Washington, DC, USA, 1991.
Pathak, R. K., Wu, W. S., and Wang, T.: Summertime $PM_{2.5}$ ionic species in four major cities of China: nitrate formation in an ammonia-deficient atmosphere, Atmos. Chem. Phys., 9, 1711–1722, doi:10.5194/acp-9-1711-2009, 2009.
Pinto, J. P., Meng, Q., Dibb, J. E., Lefer, B. L., Rappenglueck, B., Ren, X., Stutz, J., Zhang, R.: Intercomparison of nitrous acid (HONO) measurement techniques during SHARP, AGU fall meeting, San Fransisco, USA, 2010
Ren, X. R., Harder, H., Martinez, M., Lesher, R. L., Oliger, A., Simpas, J. B., Brune, W.

ACPD
12, 4679–4717, 2012

H., Schwab, J. J., Demerjian, K. L., He, Y., Zhou, X. L., and Gao, H. G.: OH and HO_2 chemistry in the urban atmosphere of New York City, Atmos. Environ., 37, 3639–3651, doi:10.1016/s1352-2310(03)00459-x, 2003.

Richter, A., Burrows, J. P., Nuss, H., Granier, C., and Niemeier, U.: Increase in tropospheric nitrogen dioxide over China observed from space, Nature, 437, 129–132, doi:10.1038/nature04092, 2005.

Ryerson, T. B., Williams, E. J., and Fehsenfeld, F. C.: An efficient photolysis system for fast-response NO_2 measurements, J. Geophys. Res.-Atmos., 105, 26447–26461, 2000.

Sander, S. P., J. Abbatt, J. R. Barker, J. B. Burkholder, R. R. Friedl, D. M. Golden, R. E. Huie, C. E. Kolb, M. J. Kurylo, G. K. Moortgat, V. L. Orkin and P. H. Wine: Chemical Kinetics and Photochemical Data for Use in Atmospheric Studies, Evaluation No. 17, JPL Publication 10-6, Jet Propulsion Laboratory, Pasadena, http://jpldataeval.jpl.nasa.gov, 2011.

Shao, M., Lu, S. H., Liu, Y., Xie, X., Chang, C. C., Huang, S., and Chen, Z. M.: Volatile organic compounds measured in summer in Beijing and their role in ground-level ozone formation, J. Geophys. Res.-Atmos., 114, D00g06, doi:10.1029/2008jd010863, 2009.

Shirley, T. R., Brune, W. H., Ren, X., Mao, J., Lesher, R., Cardenas, B., Volkamer, R., Molina, L. T., Molina, M. J., Lamb, B., Velasco, E., Jobson, T., and Alexander, M.: Atmospheric oxidation in the Mexico City Metropolitan Area (MCMA) during April 2003, Atmos. Chem. Phys., 6, 2753–2765, doi:10.5194/acp-6-2753-2006, 2006.

Sillman, S., Logan, J. A., and Wofsy, S. C.: The sensitivity of ozone to nitrogen oxides and hydrocarbons in regional ozone episodes, J. Geophys. Res., 95, 1837–1851, 1990.

Slusher, D. L., Huey, L. G., Tanner, D. J., Flocke, F. M., and Roberts, J. M.: A thermal dissociation-chemical ionization mass spectrometry (TD-CIMS) technique for the simultaneous measurement of peroxyacyl nitrates and dinitrogen pentoxide, J. Geophys. Res.-Atmos., 109, D19315, 10.1029/2004jd004670, 2004.

Streets, D. G., Fu, J. S., Jang, C. J., Hao, J. M., He, K. B., Tang, X. Y., Zhang Y. H., Wang, Z. F., Li, Z. P., Zhang, Q., Wang, L. T., Wang, B. Y., and Yu, C.: Air quality during the 2008 Beijing Olympic Games, Atmos. Environ., 41, 480–492, 2008.

Su, H., Cheng, Y. F., Shao, M., Gao, D. F., Yu, Z. Y., Zeng, L. M., Slanina, J., Zhang, Y. H., and Wiedensohler, A.: Nitrous acid (HONO) and its daytime sources at a rural site during the 2004 PRIDE-PRD experiment in China, J. Geophys. Res.-Atmos., 113, D14312, 10.1029/2007jd009060, 2008.

Thornton, J. and Abbatt, J. P. D.: Measurements of HO2 uptake to aqueous aerosol: Mass

ACPD
12, 4679–4717, 2012

accommodation coefficients and net reactive loss, J. Geophys. Res.-Atmos., 110, D08309, 10.1029/2004jd005402, 2005.

Thornton, J. A., Jaegle, L., and McNeill, V. F.: Assessing known pathways for HO_2 loss in aqueous atmospheric aerosols: Regional and global impacts on tropospheric oxidants, J. Geophys. Res.-Atmos., 113, D05303, 10.1029/2007jd009236, 2008.

van Donkelaar, A., Martin, R. V., Brauer, M., Kahn, R., Levy, R., Verduzco, C., and Villeneuve, P. J.: Global Estimates of Ambient Fine Particulate Matter Concentrations from Satellite-Based Aerosol Optical Depth: Development and Application, Environ. Health Perspect., 118, 847–855, doi:10.1289/ehp.0901623, 2010.

Volkamer, R., Sheehy, P., Molina, L. T., and Molina, M. J.: Oxidative capacity of the Mexico City atmosphere – Part 1: A radical source perspective, Atmos. Chem. Phys., 10, 6969–6991, doi:10.5194/acp-10-6969-2010, 2010.

Wang, T., Nie, W., Gao, J., Xue, L. K., Gao, X. M., Wang, X. F., Qiu, J., Poon, C. N., Meinardi, S., Blake, D., Wang, S. L., Ding, A. J., Chai, F. H., Zhang, Q. Z., and Wang, W. X.: Air quality during the 2008 Beijing Olympics: secondary pollutants and regional impact, Atmos. Chem. Phys., 10, 7603–7615, doi:10.5194/acp-10-7603-2010, 2010.

Wood, E. C., Herndon, S. C., Onasch, T. B., Kroll, J. H., Canagaratna, M. R., Kolb, C. E., Worsnop, D. R., Neuman, J. A., Seila, R., Zavala, M., and Knighton, W. B.: A case study of ozone production, nitrogen oxides, and the radical budget in Mexico City, Atmos. Chem. Phys., 9, 2499–2516, doi:10.5194/acp-9-2499-2009, 2009.

Yang, Q., Wang, Y. H., Zhao, C., Liu, Z., Gustafson, W. I. J., and Shao, M.: NOx emission reduction and its effects on ozone during the 2008 Olympic Games, Environ. Sci. Technol., 45, 6404–6410, doi:10.1021/es200675v, 2011.

Zhang, Q., Streets, D. G., Carmichael, G. R., He, K. B., Huo, H., Kannari, A., Klimont, Z., Park, I. S., Reddy, S., Fu, J. S., Chen, D., Duan, L., Lei, Y., Wang, L. T., and Yao, Z. L.: Asian emissions in 2006 for the NASA INTEX-B mission, Atmos. Chem. Phys., 9, 5131–5153, doi:10.5194/acp-9-5131-2009, 2009.

Zhang, Y. H., Su, H., Zhong, L. J., Cheng, Y. F., Zeng, L. M., Wang, X. S., Xiang, Y. R., Wang, J. L., Gao, D. F., Shao, M., Fan, S. J., and Liu, S. C.: Regional ozone pollution and observation-based approach for analyzing ozone-precursor relationship during the PRIDE-PRD2004 campaign, Atmos. Environ., 42, 6203–6218, 10.1016/j.atmosenv.2008.05.002, 2008.

Zhao, C., Wang, Y. H., and Zeng, T.: East China Plains: A “Basin” of Ozone Pollution, Environ.

ACPD
12, 4679–4717, 2012

Sci. Technol., 43, 1911–1915, 10.1021/es8027764, 2009a.
Zhao, C., Wang, Y., Choi, Y., and Zeng, T.: Summertime impact of convective transport and lightning NOx production over North America: modeling dependence on meteorological simulations, Atmos. Chem. Phys., 9, 4315–4327, doi:10.5194/acp-9-4315-2009, 2009.
Zhao, C. and Wang, Y. H.: Assimilated inversion of NOx emissions over east Asia using OMI NO_2 column measurements, Geophys. Res. Lett., 36, L06805, doi:10.1029/2008gl037123, 2009.
Zhao, C., Wang, Y. H., Yang, Q., Fu, R., Cunnold, D., and Choi, Y.: Impact of East Asian summer monsoon on the air quality over China: View from space, J. Geophys. Res.-Atmos., 115, D09301, doi:10.1029/2009jd012745, 2010.
Zhu, T., Li, X., Hu, M., Tang, X., Team CareBeijing: Air pollution characteristics before, during and after the Beijing Olympics, Epidemiology, doi:10.1097/01.ede.0000362836.37333.86, 2009.

ACPD
12, 4679–4717, 2012

Table 1. Sensitivity simulation scenarios.

Scenarios or purposes	Description
S0	Standard model setup: with full VOC chemistry, excess HONO, $\gamma(HO_2)$ = 0.02
S0a	S0 with $\gamma(HO_2) = 0$
S0b	S0 with $\gamma(HO_2) = 0.2$
S1	S0 without excess HONO
S2	S0 without aromatics
S3	S0 without excess HONO or aromatics
S3a	S3 with $\gamma(HO_2) = 0$
$P(O_3)_{senst}$	S0, S0b, S1, S2, S3, S3a constrained with 50 %, 70 %, 90 %, 110 % of observed values of NO, VOCs respectively, and both of them
$\gamma(HO_2)_{senst}$	S0 with $\gamma(HO_2) = 0$, 0.02, 0.05, 0.1, 0.15, 0.2

ACPD
12, 4679–4717, 2012

Table 2. R^2 values beteewn $P(O_3)$ and $\sqrt{Q - L_N - L_R}[NO]$, $\frac{L_{OH-VOC}}{L_{OH-NO_2}}(Q - 2PER - L_R - L_{ON})$, Q, and NO during the daytime (06:00–18:00) and afteroon (12:00–18:00).

	$\sqrt{Q - L_N - L_R}[NO]$		$\frac{L_{OH-VOC}}{L_{OH-NO_2}}(Q - 2PER - L_R - L_{ON})$		Q		NO	
	day	afternoon	day	afternoon	day	afternoon	day	afternoon
S0	0.19	0.5	0.79	0.79	0.74	0.66	0.002	0.2
S0a	0.18	0.56	0.49	0.49	0.79	0.72	0.002	0.18
S0b	0.2	0.34	0.72	0.77	0.58	0.46	0.002	0.14
S1	0.09	0.69	0.77	0.77	0.86	0.85	0.03	0.09
S2	0.14	0.26	0.77	0.79	0.49	0.34	0.01	0.06
S3	0.1	0.59	0.76	0.79	0.77	0.72	0.07	0.03
S3a	0.06	0.56	0.76	0.77	0.62	0.79	0.08	0.03

ACPD
12, 4679–4717, 2012

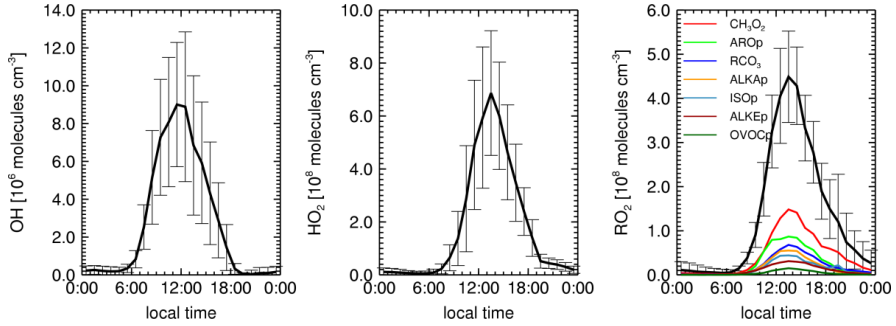

Fig. 1. Average diurnal profiles of OH, HO_2 and RO_2 (black lines) in the standard model (S0). The vertical bars show the hourly standard deviations. The color lines in the right panel show the major components of RO_2, which are described in the text.

ACPD
12, 4679–4717, 2012

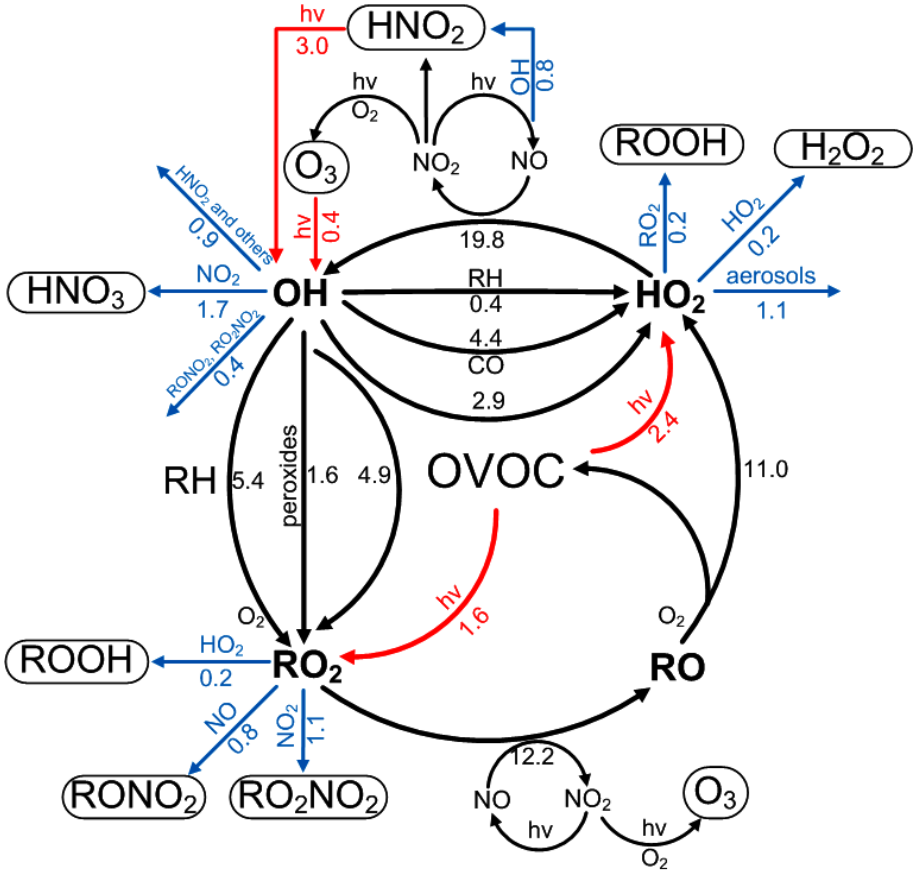

Fig. 2. Daytime (06:00–18:00) average budgets of RO_x radicals. Primary RO_x sources and sinks are in red and blue, respectively. The production and loss rates are in ppbv h^{-1}.

ACPD
12, 4679–4717, 2012

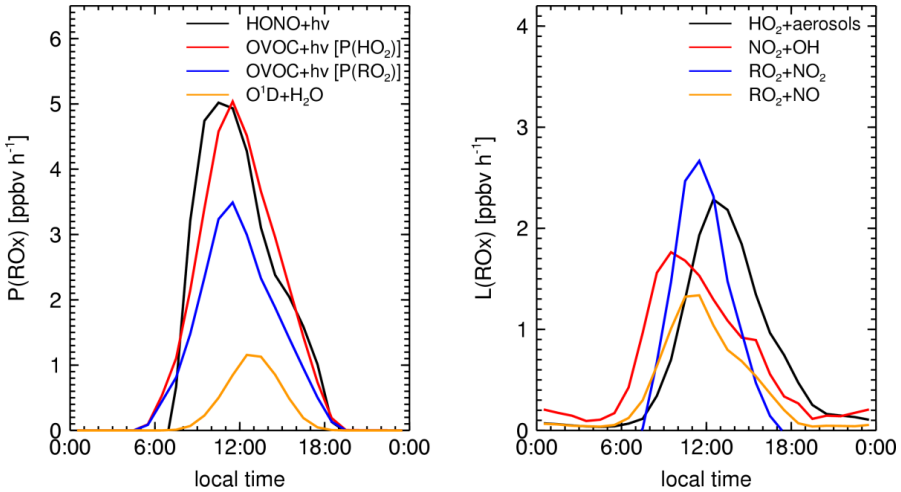

Fig. 3. Average diurnal profiles of major RO_x primary sources and sinks.

ACPD
12, 4679–4717, 2012

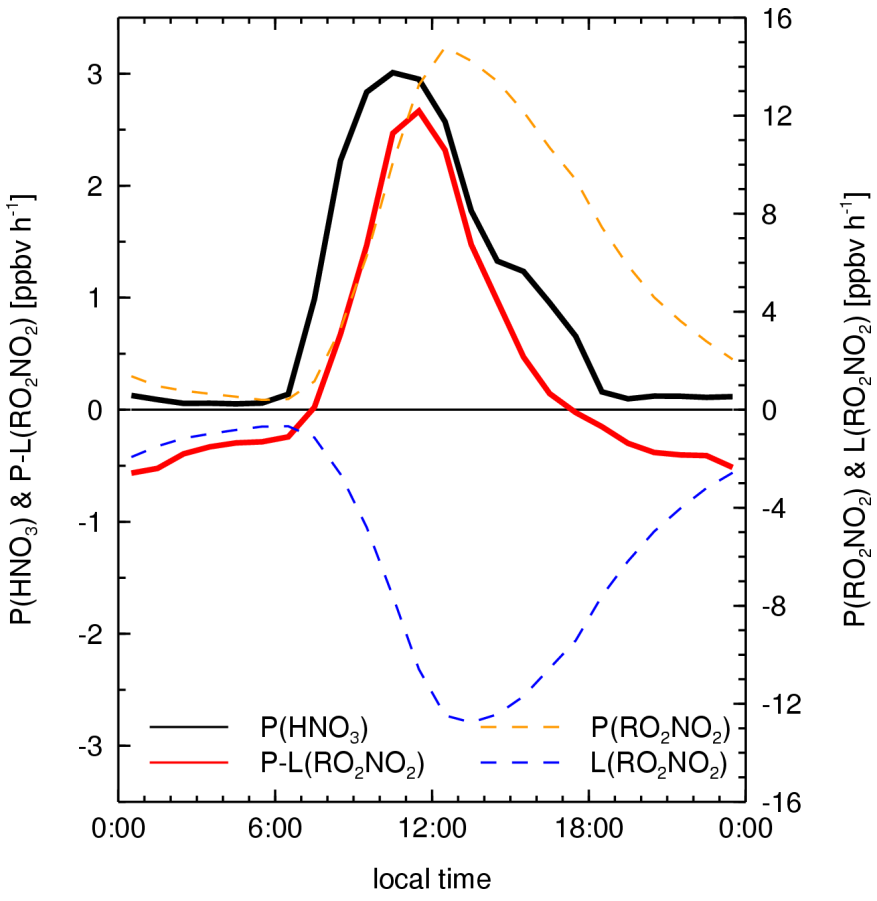

Fig. 4. Average diurnal profiles of net formation rates of PANs and HNO_3. Production and loss rates of PANs are also shown.

ACPD
12, 4679–4717, 2012

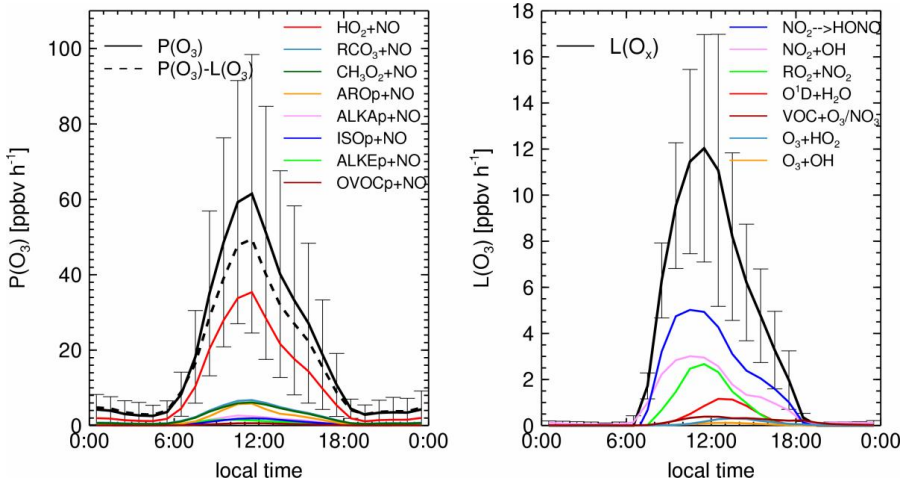

Fig. 5. Average diurnal profiles and breakdowns of O_3 production (left) and loss rates (ppbv h^{-1}) (right). The vertical bars show the standard deviation.

ACPD
12, 4679–4717, 2012

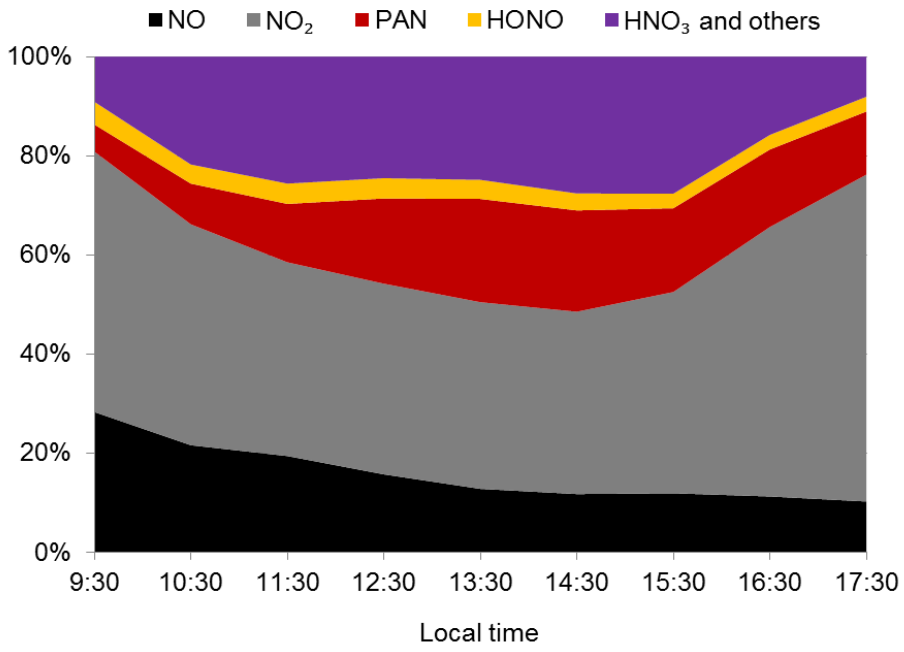

Fig. 6. Daytime evolution of NO_y components.

ACPD
12, 4679–4717, 2012

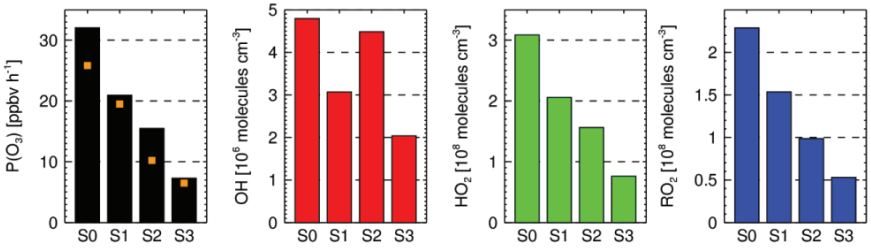

Fig. 7. Daytime average O_3 production rates and concentrations of OH, HO_2, and RO_2 under scenarios S0, S1, S2, and S3. The yellow squares show the net O_3 formation rates ($P(O_3)$-$L(O_3)$).

ACPD
12, 4679–4717, 2012

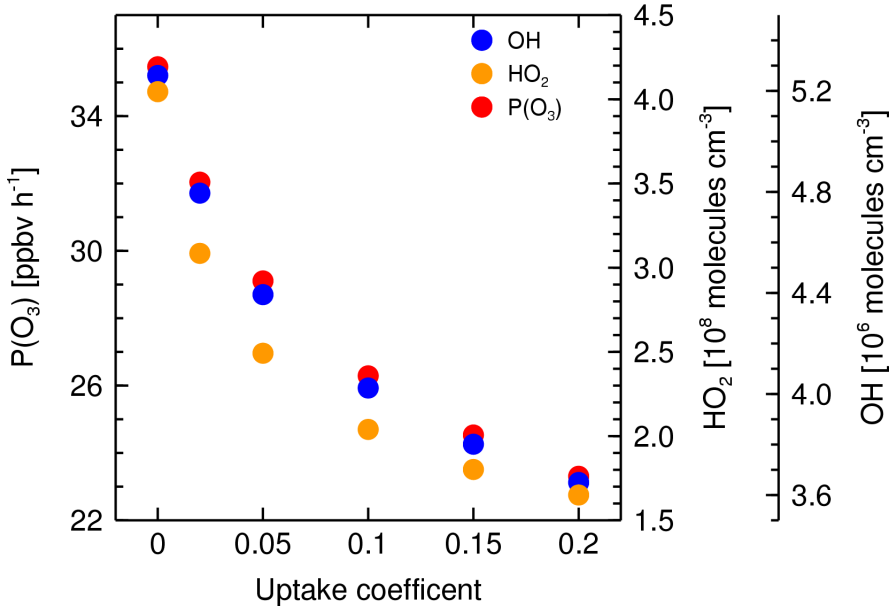

Fig. 8. Daytime average HO_2, OH and $P(O_3)$ as a function of $\gamma(HO_2)$.

ACPD
12, 4679–4717, 2012

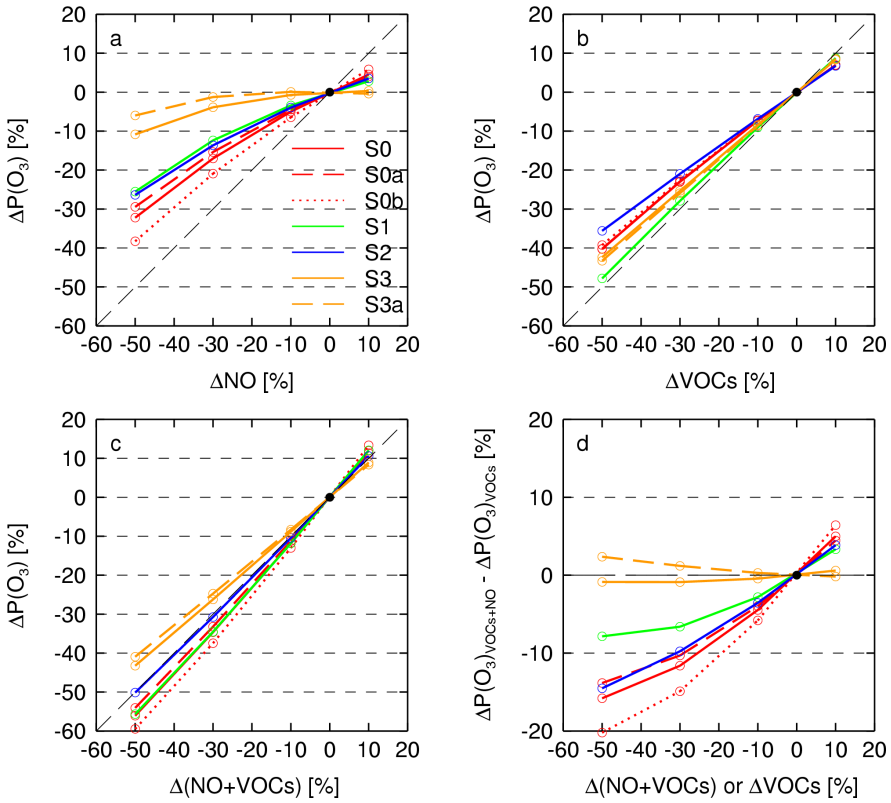

Fig. 9. Changes of O_3 production ($\Delta P(O_3)$) as a function of NO, VOCs, and both under different scenarios in Table 1.

ACPD
12, 4679–4717, 2012

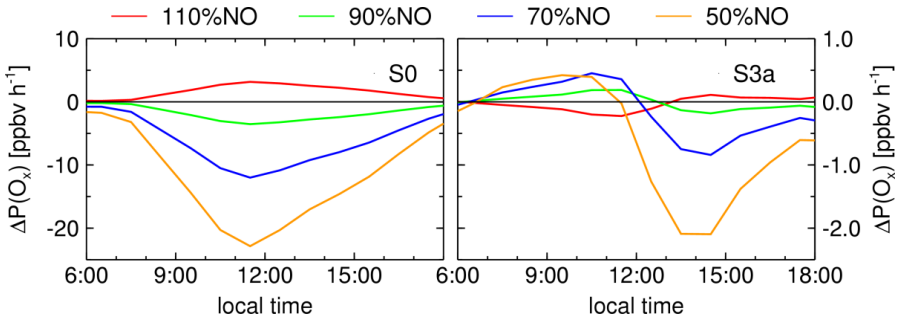

Fig. 10. Hourly $\Delta P(O_3)$ due to NO changes under S0 and S3a.

ACPD
12, 4679–4717, 2012